Journal of Materials Chemistry A

Accepted Manuscript

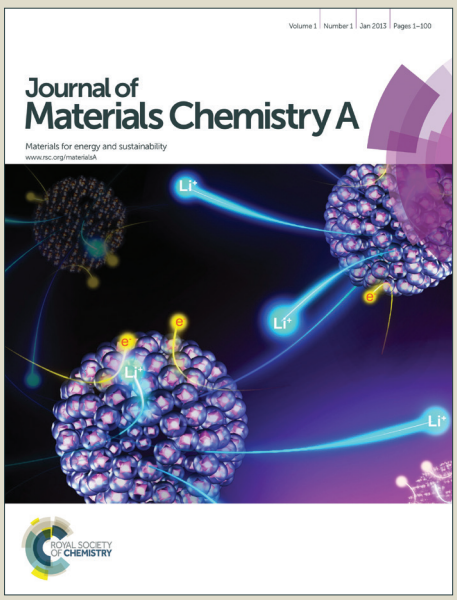

ROYAL SOCIETY OF CHEMISTRY

www.rsc.org/materialsA

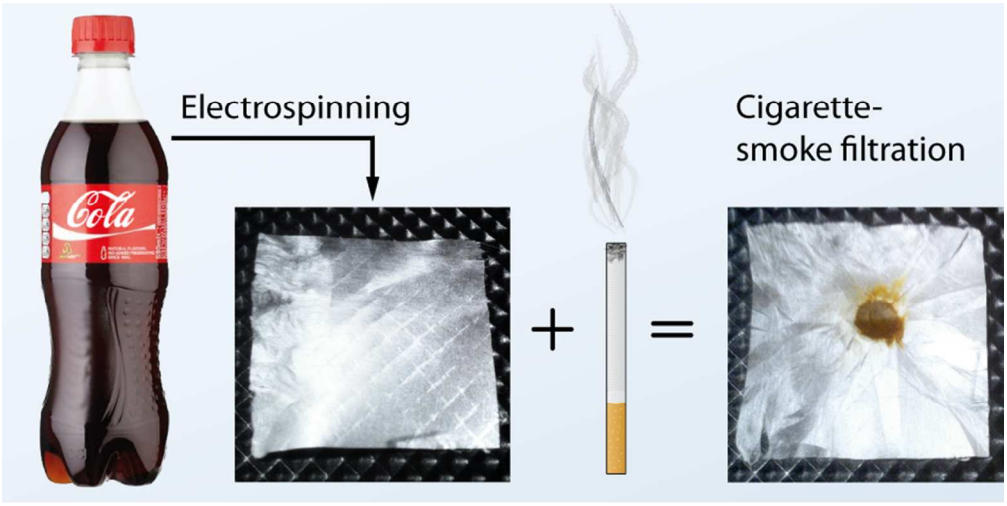

Regeneration of used PET bottles via electrospinning, into high performance membranes for smoke filtration.

Journal Name

RSCPublishing

ARTICLE

Electrospinning of recycled PET to generate tough mesomorphic fibre membranes for smoke filtration

Cite this: DOI: 10.1039/x0xx00000x

I. N. Strain[a], Q. Wu[b], A. M. Pourrahimi[b], M. S. Hedenqvist[b], R. T. Olsson[b,*], and R. L. Andersson[b,*]

Received 00th January 2012,
Accepted 00th January 2012

DOI: 10.1039/x0xx00000x

www.rsc.org/

Abstract

Tough fibrous membranes for smoke filtration have been developed from recycled polyethylene terephthalate (PET) bottles by solution electrospinning. The fibre thicknesses' were controlled from 0.4 to 4.3 µm by adjustment of the spinning conditions. The highest fibre strength and toughness were obtained for fibres with an average diameter of 1.0 µm, 62.5 MPa and 65.8 MJ/m^3, respectively. The X-ray diffraction (XRD) patterns of the fibres showed a skewed amorphous halo, whereas the differential scanning calorimetry (DSC) results revealed an apparent crystallinity of 6–8 % for the 0.4- and 1-µm fibres and 0.2% crystallinity for the 4.3-µm fibres. Heat shrinkage experiments were conducted by exposing the fibres to a temperature above their glass transition temperature (T_g). The test revealed a remarkable capability of the thinnest fibres to shrink by 50 %, which was in contrast to the 4.3-µm fibres, which displayed only 4 % shrinkage. These thinner fibres also showed a significantly higher glass transition temperature (+15 °C) than that of the 4.3-µm fibres. The results suggested an internal morphology with a high degree of molecular orientation in the amorphous segments along the thinner fibres, consistent with a constrained mesomorphic phase formed during their rapid solidification in the electric field. Air filtration was demonstrated with cigarette smoke as a model substance passed thru the fibre mats. The 0.4-µm fibres showed the most effective smoke filtration and a capacity to absorb 43x its own weight in smoke residuals, whereas the 1-µm fibres showed the best combination of filtration capacity (32x) and mechanical robustness. The use of recycled PET in the form of nanofibres is a novel way of turning waste into higher-value products.

Introduction

Useful recycling of plastic polymer waste is a growing concern over the entire globe. In the United States in 2012, 32 million tons of plastic waste were generated, amounting to 12.7 % by weight of the total municipal solid waste,[1] but about twice that if considering the volume[2]. Only 9 % of this plastic waste was recovered for recycling,[1] ca. 30 % of which was related to the collection of used poly(ethylene terephthalate) (PET) bottles.[3] These post-consumer PET bottles are nowadays highly valued in manufacturing since they are inexpensive compared to virgin PET, which would have an equivalent market price of ca. 150 million USD if no PET would be recycled in the USA.[4] The current market for recycled PET ranges from engineering plastics, automobiles, packaged foods, containers, fleece fabric, and different kinds of film.[5, 6] However, virgin PET also has additional use in applications such as protective clothing, membranes, vascular grafts, tissue scaffolding, and filtration.[6, 7] Thus, recycled PET could be an ideal cost-effective choice in a variety of applications.

Bottle-grade PET exists as a semi-crystalline thermoplastic with high impact and tensile strength, chemical resistance, and a reasonable thermal stability,[8, 9] but since recycled PET has been in contact with a variety of substances and environments, applications in a biological setting are not suitable. This fact, in addition to the growing concerns on environmental air pollution,[10] means that filtration is one of the most promising application for recycled ultrathin PET fibres. Nonwoven fabrics of PET could here play a momentous role in dust filtration because of their porous structure and low cost of manufacturing in combination with its unique mechanical properties.[10] Utilization of recycled PET bottles for the manufacture of profitable filtration products would help to offset the cost of recycling and encourage the collection of post-consumer PET bottles. The PET polyester is also particularly marketable for recycling since it is one of the most easily identifiable thermoplastics since almost all beverage bottles are made of PET.

An increasingly popular technique for the production of non-woven membranes is electrospinning, which is one of the most rapidly growing industrial polymer processing methods for the production of ultrathin fibres. Studies on the electrospinning of PET exist, but only one published study concerns the electrospinning of recycled PET,[9] where electrospinning from melt was applied to prepare ca. 30 µm thick fibres. Polymer melt spinning is a useful technique to handle thermoplastics when traces of other plastics are possibly present as long as the polymers show melt characteristics that enable them to mix properly at a given process temperature. The drawback is the considerable amounts of heat (energy) required to process the material, and inferior mechanical properties with repeated heating cycles.[11, 12] Another limitation of the electrospinning of polymer melts is the relatively high viscosity of the spun material, making it difficult to produce very thin uniform fibres.[13] A possible alternative advantageous method would be to carry out the electrospinning of recycled

PET from solvents, since it allows for unprecedented control of fibre morphology. The solvents could be recycled by process-coupled condensation units, with the additional cost for this offset by the thermal energy savings and the benefits of separation of fillers after precipitation and sedimentation.

In this present study, solvent-based electrospinning was used to produce recycled PET micro- and nanofibres for application-oriented research. The possibility of producing large quantities of continuous ultrafine fibres with a thickness ca. 2 orders of magnitude smaller than previously reported is shown.[14] Fibre morphology and mean diameter were studied in relation to the flow rate and concentration of recycled PET. The electrospun fibre properties were determined by cold-field-emission scanning electron microscopy (FE-SEM), infrared spectroscopy (IR), tensile testing, X-ray diffraction (XRD), and differential scanning calorimetry (DSC). The prepared fibres were collected as aligned fibre mats for mechanical testing in a micromechanical stage, and as randomly oriented fibres in isotropic fibre mats. The fibre mats were demonstrated as filters for airborne substances such as polycyclic aromatic hydrocarbons (PAH), persistent organic pollutant (POP) and most recently fine particulate matter (nanoparticles) since the effect of these in our environment is a current concern.[15] In this study cigarette smoke was chosen as a model substance, as it contains several thousands of components, which includes PAH, POP and ca. 5 % particulate matter.[16, 17] The results pave the way for supplementary studies on the optimization of these ultrafine membranes for use in nanofiltration and other applications in consumer and industrial products.

Experimental

Preparation of polymer solution for electrospinning

Recycled polyethylene terephthalate (PET) was obtained from Coca Cola bottles (500 mL) collected from the same production batch (Coca-Cola Enterprises Sweden AB). The PET bottles were produced from at least 99.8 wt% PET without plasticizers, as determined from the data-sheet from the manufacturer. The molecular weight of this type of PET, which is commonly used during the production of PET bottles, typically lies in the range of 30–80 kDa.[8] All the bottles were cleaned and rinsed with pure ethanol prior to drying, followed by shredding into 5x5 mm^2 small pieces. Trifluoroacetic acid (TFA, *Reagent Plus,* 99 %) was purchased from Sigma-Aldrich and dichloromethane (DCM, ACS Grade Stabilized, 99.5 %) was purchased from VWR International. A mixture of TFA and DCM in a ratio 70/30 by weight was prepared. The recycled PET was then added to the solvent mixture at concentrations of 10, 15, and 20 wt%. Solutions were mixed for 24 h to ensure complete dissolution of the PET at a temperature of 20 °C.

Electrospinning of unaligned fibres

The polymer solutions were fed at different rates (20, 10 and 5 $\mu L \cdot min^{-1}$) from a 5 mL solvent resistant syringe through a polytetrafluoroethylene tube attached to a steel needle (inner diameter 0.60 mm) mounted 25 cm above the collection plate. An electric potential between 7–12 $kV \cdot m^{-1}$ (depending on the concentration of PET and flow rate) was applied by adjusting the voltage from the needle to the collection plate. The faster the flow rate, the greater was the voltage required for spinning.[18] All samples were spun for 20 min to ensure that a substantial amount of fibres could be obtained for FE-SEM and IR-spectroscopy analysis.

Electrospinning of aligned fibres

The preparation of the aligned fibres was identical with that of the unaligned fibres except that solutions were fed at a fixed flow rate and voltage. The 10 and 15 wt% PET concentrations were spun with a flow rate of 5 $\mu L \cdot min^{-1}$, whereas the 20 wt% concentration was spun with a flow rate of 10 $\mu L \cdot min^{-1}$, as these conditions gave the most uniform fibres. The fibres were collected on a rotating alignment drum (diameter = 50 mm) rotating at 2000 rpm at the same spinning distance (25 cm) as the unaligned fibres. The total spin time was varied depending on the PET concentration of the sample (10 wt% spun for 4 h, 15 wt% for 2 h, and 20 wt% for 1 h) in order to produce fibre mats of similar thicknesses.

Tensile Testing

Fig. 1 shows the micromechanical tensile testing stage with a mounted PET fibre mat. The tensile tests were performed according to a previously reported Template Transfer Method (TTM).[19, 20]

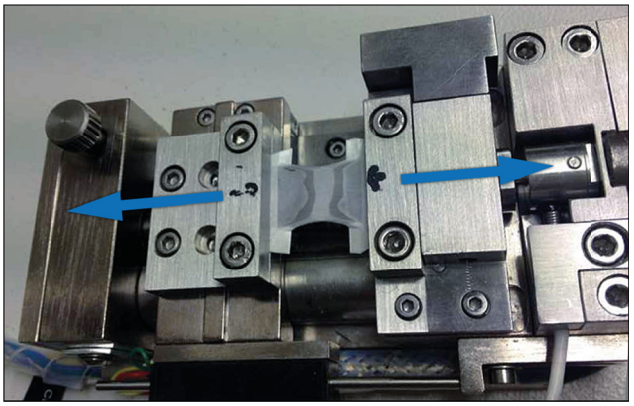

Fig. 1. Photograph of the Micromechanical tensile stage with mounted PET fibres (at ca. 100 % strain) according to the Template Transfer Method (TTM).[19]

Four pieces of fluorinated ethylene propylene release films (thickness = 76 µm) were first secured along the centre of the alignment drum. Aluminium foil templates (thickness = 30 µm) with a cut out window (length = 5 mm, width = 10 mm) were then attached over the release films, which were attached to the drum with copper tape (thickness = 66 µm). The cut-out window allowed fibre testing on a Deben Microtest micromechanical stage (Fig. 1). Before removal from the alignment drum, fibres were fixed to both sides of the window using alkoxy-ethyl-cyanoacrylate (Loctite 460, Hennkel AG & Co. KGaA, Germany). Once secured in the tensile stage, the side panels of the window were cut (while leaving the fibres intact). The length, width, and thickness of a piece of PET bottle was measured and weighed and the density of the PET was determined to be 1.37 $g \cdot cm^{-3}$. This value was in agreement with the previously reported density of bottle-grade PET (which is also close to that of amorphous PET)[21] and was used to calculate the thickness of the fibre mats after electrospinning,

i.e. by weighing a known area of the fibre mat taken adjacent to the template on the collection drum. The tensile strength was taken as the highest stress supported during the test, the Young's modulus was taken as the initial linear slope of the stress–strain curve and the toughness was calculated as the total area under the stress–strain curve.

Determination of fibre size and morphology

Using detailed scanning electron micrographs, 200 fibres were measured from each spun sample of aligned and unaligned fibres. The angular deviation of aligned fibres was calculated from a minimum of 50 fibres from each spun sample. For these measurements, a Hitachi S-4800 cold-field-emission scanning electron microscope (FE-SEM) was used in conjunction with a thin Pt/Pd 60/40 coating, (10 s at 80 mA) in a Cressington 208HR high-resolution sputter.

The molecular draw ratio of each aligned fibre mat (20×20 mm^2 cut-outs) was evaluated from their shrinkage upon heating to 150 °C, over a temperature-controlled aluminium surface.

Infra-red Spectroscopy (IR)

All IR spectroscopy measurements were performed on a Perkin-Elmer Spectrum 2000 using a 1 cm^{-1} scan step and a single reflection attenuated total reflectance stage (ATR) MKII Golden Gate unit.

X-ray diffraction (XRD)

The electrospun samples were prepared as thick sample discs to obtain the highest possible diffraction intensity, *i.e.* by compressing the fibres in a Specac circular dye (diameter 10 mm) for 1 min and 100 kN at room temperature. X–ray diffractograms on samples were taken at room temperature using a PANalytical X'pert Pro MPD diffractometer with a Cu-Kα source (wavelength 1.5418 Å) at a step size of 1 arcmin (2θ) and scan step time of 51 s.

Differential scanning calorimetry (DSC)

Thermograms of fibres were obtained with a temperature- and energy-calibrated Mettler–Toledo DSC1. Each sample was weighed at 2.0 ± 0.1 mg, enclosed in a 100 mL standard aluminium crucible with one hole in the cover. The samples were heated from 30 °C to 300 °C at a rate of 10 °C·min^{-1} under a nitrogen atmosphere at a gas flow rate of 50 µL·min^{-1}, and allowed to rest for 5 min before subsequent cooling at 10 °C min^{-1}. The degree of crystallinity ($X_{c,DSC}$) was calculated, under the assumption that the morphology of amorphous regions before cold crystallisation and after melting are the same, from the equation:[22]

$$X_{C,DSC} = \left(\Delta H_f - \Delta H_c\right)/\Delta H_f^0 \qquad \text{(Eq. 1)}$$

Where ΔH_f is the enthalpy of fusion, ΔH_c is the enthalpy of cold crystallization, assessed directly from DSC thermograms, and ΔH°_f (136 J·g^{-1}) is the enthalpy of fusion of 100% crystalline PET.[23]

Smoke Filtration

To determine the smoke filtering properties of the fibre mats with different fibre diameters, the mats were evaluated by securing them over a glass tube (9 mm diameter) fitted within a tubular system for smoke transportation and testing (see Fig. 7c). A cigarette (Marlboro Gold, Philip Morris International) with its filter removed was fitted into the other end of the glass tube at a distance of 25 mm from the fibre mat. The specific surface area of each filter was calculated from the measured average diameter (from SEM) of the fibres. IR-spectroscopy was employed to determine what sort of components were absorbed, small amounts of smoke were used for this purpose, *i.e.* 2 mL of smoke was passed through each mat for each µg of fibre mat present, at a rate of ca. 100 mL·s^{-1}. The filtration capacity was measured gravimetrically as the total mass uptake after exposure to an excess of cigarette smoke (1000 mg of tobacco for each mg of filter), a comparison to the commercial filter tip used in the original cigarette was made using the same proportions of tobacco to filter.

Results and Discussion

Morphology and composition of electrospun recycled PET-fibres

Fig. 2a to c shows the result of increasing the concentration of PET in the solvent carrier. By adjusting the concentration, the average fibre diameter could be precisely controlled, while the fibre morphologies were almost unaffected and showed continuous long fibres with smooth surfaces. The insets in the micrographs show the size distribution of the fibres, obtained by measuring the diameters of at least 200 fibres for each sample. The average fibre diameters at these flow rates increased from 0.41 µm (± 0.12 µm, *i.e.* ± 30 %) at 10 wt%, to 1.0 µm (± 0.19 µm, *i.e.* ± 19 %) at 15 wt%, to 4.3 µm (± 0.34 µm, *i.e.* ± 8 %) at 20 wt% PET. The relative standard deviation was largest for the thinner fibres and decreased with increasing fibre thickness, possibly due to the lower viscosity and high surface tension of the electrospun solutions for these samples, as previously reported.[24] Fig. 2d shows the relationship between the fibre diameter and the PET concentration at different flow rates. A flow rate three times as high (at a given concentration) had only a marginal effect on the thickness of the fibres. For all the evaluated formulations and flow rates, the fibres with greatest uniformity were always prepared at the lowest spinnable flow rate (5 µL·min^{-1} for 10 and 15 wt% PET, 10 µL·min^{-1} for 20 wt% PET), Fig. 2 a–c. For ease of reference, the above fibres are hereafter referred to by their approximate diameters: 0.4, 1.0 and 4.3 µm.

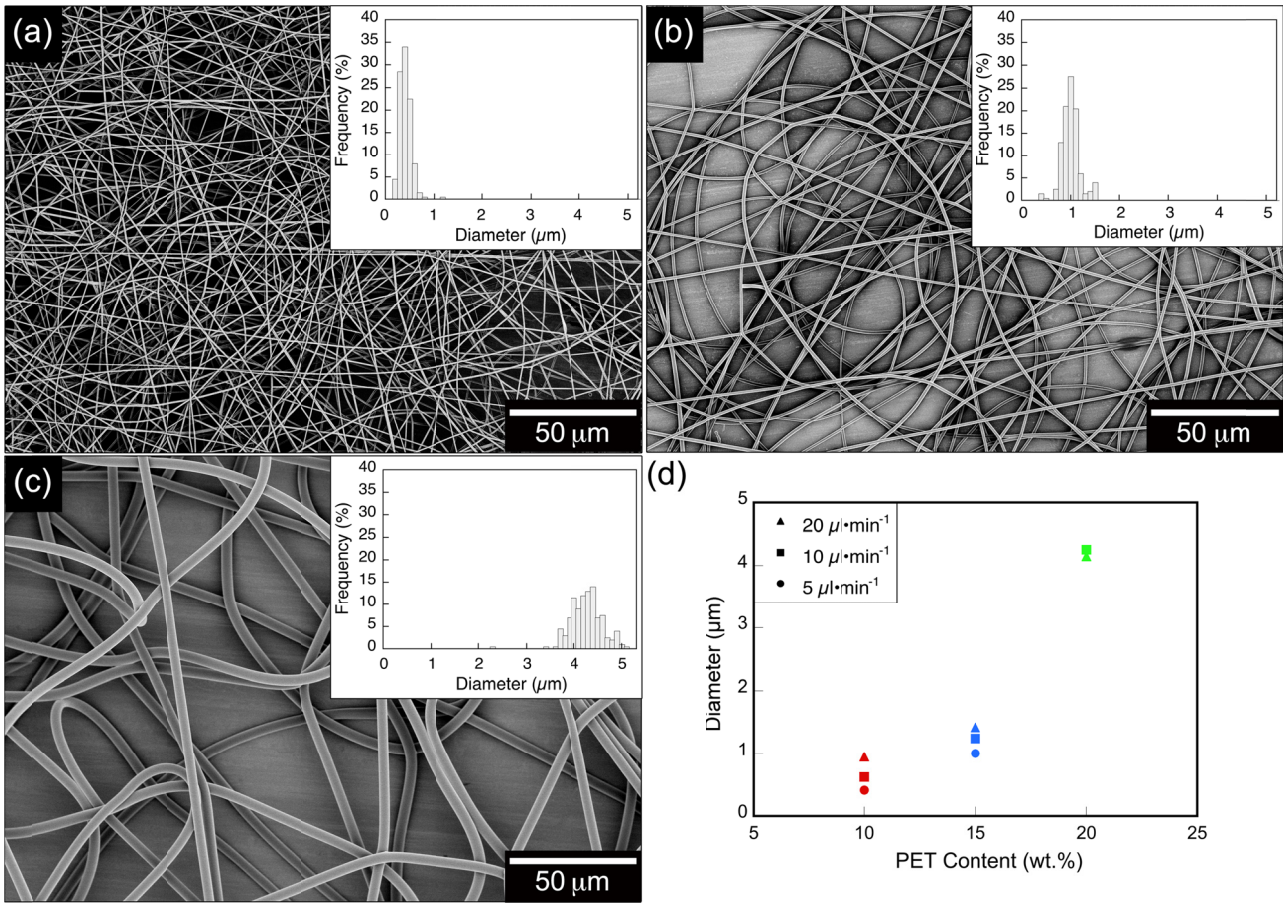

Fig. 2. Electron micrographs show the un-aligned electrospun fibres spun from solutions with different concentrations of PET (a): 10, (b): 15, (c): 20 wt%, with the same flow rates as used for tensile testing (a: 5, b: 5, c: 10 μL·min^{-1}), insets show the fibre diameter distributions, (d) shows the average fibre diameter spun at different flow rates (μL·min^{-1}) as a function of PET concentration in the electrospinning solutions.

Fig. 3 shows the acquired fibre IR-spectra for the electrospun fibres together with the original bottle PET. The analysis was made to also ensure complete TFA/DCM evaporation in all samples (only 1.0 μm fibres are shown). The four major peaks associated with the inherent structure of the polyethylene terephthalate were the terephthalic acid ester C=O group at 1714 cm^{-1}, the asymmetric C–C–O and the O–C–C stretching at 1240 and 1092 cm^{-1}, respectively, and the C-H wagging vibrations from the aromatic structures at 722 cm^{-1}. Trifluoroacetic acid would, if present, be visible within the 1250–1180 cm^{-1} region due to the C–F stretching modes (1244, 1240 and 1199 cm^{-1}),[25] whereas the dichloromethane C–Cl symmetric and asymmetric stretching should appear at 874 and 771 cm^{-1}. Among these peaks, only those of 1199, 874 and 771 cm^{-1} could be used to assess trace solvents remaining in the prepared fibre mats, due to the overlapping nature of the remaining peaks. However, none of these peaks showed any significant difference from those of the spectra for the PET samples cut from the original bottle. This PET bottle displayed a minor peak at 1340 cm^{-1} and a slightly smaller intensity of the peaks in the 3100–2800 cm^{-1} region.

In summary, the electrospinning from solution allowed the regeneration of the PET polymer as 0.4, 1.0 and 4.3 μm thick continuous fibres without any trapped solvent phases or apparent degradation of the original material.

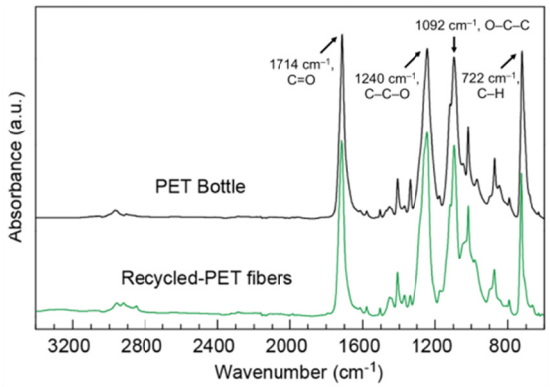

Fig. 3. IR-spectra of the 1.0 μm thick electrospun PET fibres and of the original PET bottle. The fibres were analysed 30–60 min after electrospinning to ensure that no solvent remained after this time period, i.e. prior to performing other measurements. All electrospun fibres showed the same IR-spectra.

Tensile Testing

Tensile testing was conducted on all the prepared fibres as aligned fibre mats, shown in Fig 3. The fibres had an average angular deviation of 12.4º, as concluded from FE-SEM analysis. As the fibre diameter decreased, an increase in strength and in Young's modulus was observed. This could be explained by a higher degree of molecular alignment when thinner fibres were produced in the electrical field, due to the increased fibre stretching.[26] The strain at break is usually reduced when the strength and modulus increase, but, the results contradicted this trade-off with a positive correlation between strength and strain at break, as shown in Fig. 4, *i.e.* the strongest fibres also had the highest strain at break. Of the different fibres tested, the 1.0 µm fibres showed the best combination of mean tensile strength (62.5 MPa), modulus (1.39 GPa) and toughness (65.5 MJ·m^{-3}), Fig 4. The 0.4-µm fibres had a similar strength and a higher modulus, but a significantly lower elongation at break. The fibres with a diameter of 4.3 µm had a much lower tensile strength (-87 %), lower modulus (-89 %) and lower toughness (-97 %), than the 1.0 µm fibres, Fig. 5.

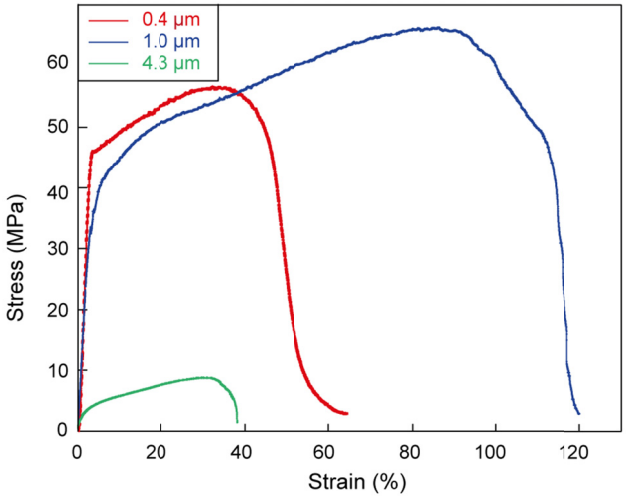

Fig. 4. Tensile stress-strain curves for the 0.4, 1.0 and 4.3 µm fibre mats.

A comparison between the 1.0 µm fibres (*i.e.* low density fibre mats) and that of bottle-grade PET (tensile strength of ca. 79 MPa, Young's modulus of ca. 2.8 GPa and elongation at break of ca. 70 %)[27] showed that the 1.0 µm fibres had only marginally lower strength and modulus but a significantly higher strain at break, *i.e.* a higher toughness. The toughness of the fibre mats was comparable to that of amorphous biaxially oriented films of PET, pre-drawn to a draw ratio of ca. 3–4.[28]

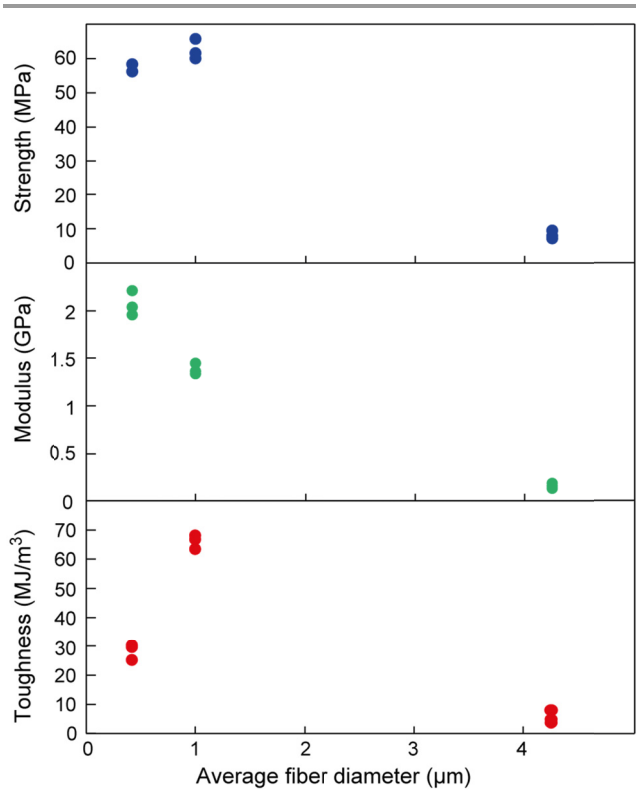

Fig. 5. The mechanical properties of the 0.4, 1.0 and 4.3 µm fibre mats as a function of average fibre diameter.

Veleirinho *et al.*[6] measured the mechanical properties along only lightly oriented electrospun fibre mats (spun virgin PET and by using the same solvent ratios as in the present study) with fibre diameters of ca. 0.6 µm. The stiffness, strength and extensibility (strain at break) were, respectively, 50–60 MPa, 1–2 MPa and 20–40 %. These properties were significantly lower than those of the present fibre mats, showing the importance of fibre alignment when evaluating the fibre properties. Commercial single melt-spun PET filaments without additional post-drawing have a stiffness, strength and extensibility on the order of 2–14 GPa, 170–550 MPa and 45–300 %.[29, 30] Post-drawn PET have been reported to have a stiffness and strength of 15 GPa and 1100 MPa, but at the expense of much inferior extensibility when compared to the present fibres.[31] Hence the conclusion from this comparison is that electrospinning PET at the present conditions does not create the same amount of high molecular orientation as in the strongest commercially post-drawn fibres. Instead the mechanical properties of the present as-spun fibre are comparable with as-spun single PET fibre filaments.

Crystal structure and molecular morphology (XRD and DSC)

Fig. 6a shows X–ray diffractograms of the PET bottle and the electrospun fibre mats. Semi–crystalline PET typically shows characteristic crystalline XRD-peaks at 2θ = 16.1, 17.5, 21.5, 22.7, 24.0, 26.1, 27.8, and 32.5°, corresponding to the: $0\bar{1}1$, 010, $\bar{1}11$, $\bar{1}10$, 011, 100, 021, 002, $1\bar{1}1$ and 101 crystal planes,[23] and a broad amorphous halo at 10–35°.[32-34] As seen in Fig. 6a, the diffractogram of the PET bottle showed only one relatively wide single diffraction peak at 25.5°, corresponding

to the (100) crystal plane, together with an amorphous halo at slightly lower angles. Nunes *et al.*[34] ascribed this particular semi–crystalline structure of PET bottles to the biaxial molecular orientation achieved in the bottle wall during blow moulding. The electrospun fibres displayed broader halos with centres at 22–23° and the absence of the peak at 25.5°, indicating that they consisted mainly of amorphous material. Hadjizadeh *et al.*[33] reported a similar lack of crystallinity in electrospun samples and attributed this to the rapid solidification of stretched PET chains. The solidification rate at the conditions used in the present study was ca. 1–10 milliseconds, which is much shorter than the time frame of ca. 50 s required for the crystallization of PET at a cooling rate of 100 °C/min.[35] However, it is also known that PET can form a mesomorphic phase (oriented amorphous phase) which does not reveal itself clearly in the diffractograms.[36] The formation of an oriented mesomorphic phase inside electrospun PET fibres has also been proposed by Wang *et al.*[24] Keum *et al.* showed that the presence of this oriented amorphous phase reveals itself as a skew in the amorphous halo.[37] This sort of skewed (unsymmetrical) amorphous halo was most noticeable in the case of the 0.4 and the 1.0-µm fibres, as can be seen in Fig. 6a.

The existence of an oriented molecular morphology inside the fibres was verified by a shrinkage test, where the different fibre mats were heated to a temperature of 150 °C. The shrinkage in the fibre direction was 54 % for the 0.4 µm and 43 % for the 1.0 µm fibres, whereas the shrinkage for the 4.3-µm fibres was only ca. 4 % (Table 1). This confirmed that there was a molecular orientation, since shrinkage of 54 % in the fibre direction would require an initial molecular draw ratio of 2.2 or more, and complete relaxation could not be expected due to molecular hysteresis. Similar draw ratios have previously been observed in other electrospun polymers, measured by infra-red dichroism spectroscopy.[38]

Table 1. Thermal properties and shrinkage upon heating for the PET.

Sample	T_g (°C)	$X_{C,DSC}$ (%)	Shrinkage (%)
PET Bottle	N/A	21.2	11 (∥), 41 (⊥)
Fibre 0.4 µm	81.0	7.9	54
Fibre 1.0 µm	80.5	6.0	43
Fibre 4.3 µm	66.4	0.2	3.6

The data show shrinkage in the fibre direction and for the original bottle, parallel (∥) and perpendicular (⊥) to the height of the bottle.

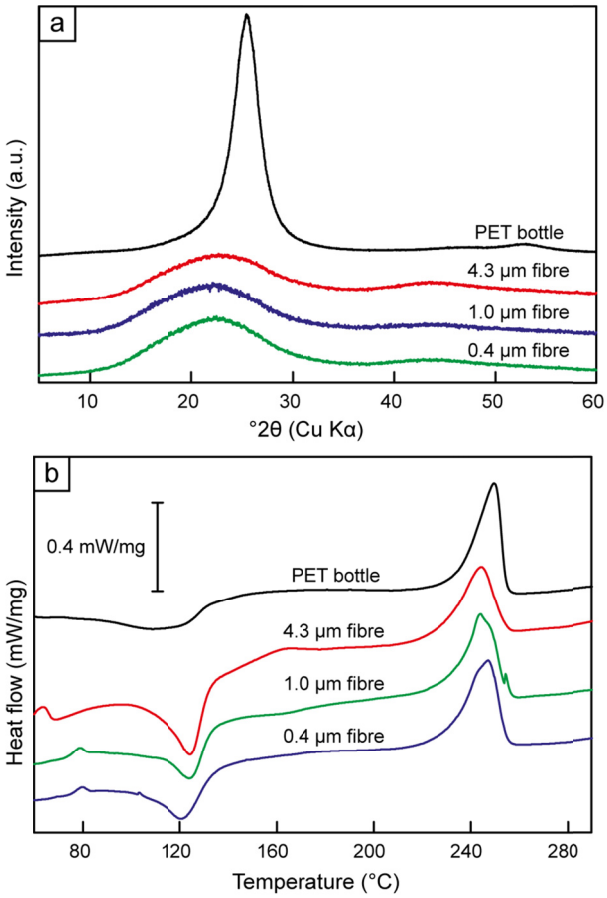

Fig. 6. X-ray diffractograms (a) and DSC thermograms (b) for the original PET bottle and fibres spun to different diameters.

The existence of a mesomorphic phase in the two thinnest fibres was further verified by the DSC analysis. Fig. 6b shows the heating thermograms of the PET bottle and the electrospun fibres with diameters from 0.4 µm to 4.3 µm. No significant difference in crystallisation temperature during heating (122 ± 2 °C) or melting point (247 ± 3 °C) could be observed between the fibre samples and the original PET bottle. The glass transition temperature (T_g) and degree of apparent crystallinity ($X_{c,DSC}$) as calculated by Eq. 1, did however show significant differences for the different samples, see Table 1.

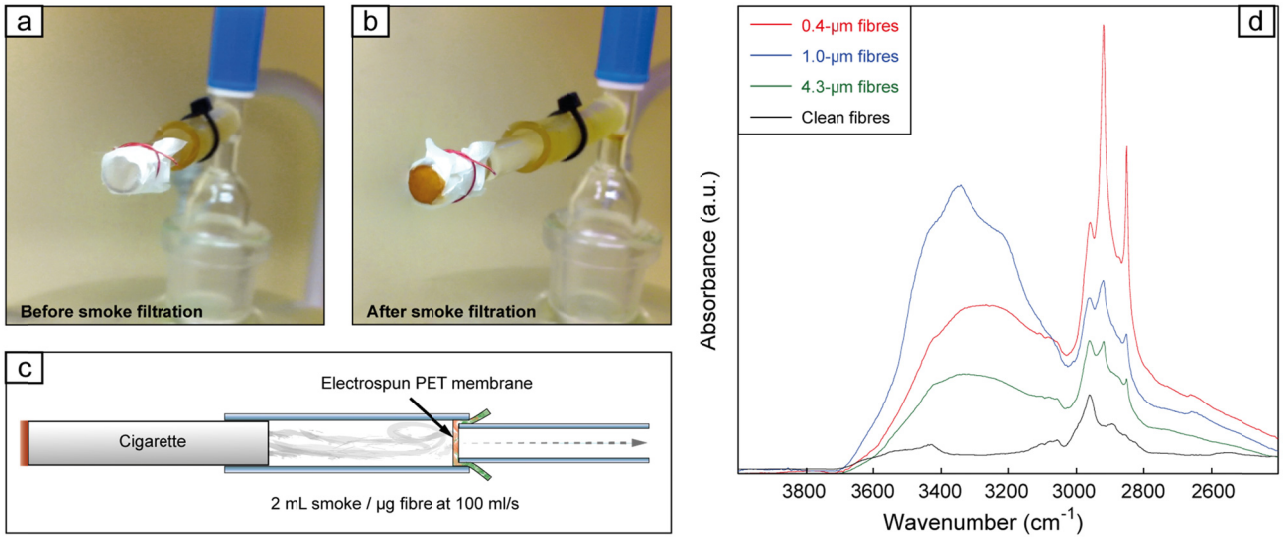

Fig. 7. Photographs of fibre mats (a) before and (b) after smoke filtration testing (1.0 µm diameter), conducted according to the scheme shown in (c). IR-spectroscopy (d) of a clean fibre mat compared to that of smoke-exposed fibre mats with average fibre diameters of 0.4, 1.0 and 4.3 µm.

The fibre mats consisting of 0.4 µm and 1.0 µm diameter fibres showed the highest T_g (80.5–81.0 °C, Table 1). This higher T_g was consistent with a more constrained/stretched amorphous phase, and the much greater shrinkage observed when these fibres were heated.[39] On the other hand, the 4.3-µm fibres showed a T_g of only 66.4 °C, which was consistent with almost no shrinking (3.6 %) of these fibres. The thermogram of the PET bottle (Fig. 6b) showed no clear glass transition due to the smaller amount of amorphous material in the original PET bottle which had a 21.2 % crystalline content.

The 4.3-µm fibres showed no significant crystallinity (0.2 %), whereas the 0.4 and 1.0 µm fibres showed an apparent degree of crystallinity of 6–8 %, Table 1. The inconsistency with the X-ray diffractograms in Fig. 6a stems from the fact that Eq. 1 assumes that the amorphous morphology before crystallisation and after melting are the same. This was not the case for the 0.4 and 1.0 µm fibres, since they initially contained a highly oriented amorphous morphology, *i.e.* a mesomorphic phase, and the change in enthalpy to the crystalline phase was thus less than that of an un-oriented amorphous material (*e.g.* the 4.3 µm fibres). On the macroscopic scale, this can be interpreted as meaning that there were local regions, smaller than the detection limit of XRD (ca. 3 nm),[39-42] with a greater ordering of PET molecules than in the completely amorphous counterpart. None of the fibres contained any conventional PET crystals and they were considered to be completely amorphous. However, in the case of the two thinnest fibres, a large degree of molecular orientation existed, which was higher than the molecular orientation in the commercial semi-crystalline PET bottle.

Influence of molecular morphology on mechanical properties

The higher modulus and tensile strength of the two thinnest fibres (0.4 and 1.0 µm), than of the 4.3 µm fibres was attributed to the greater amount of local regions with intensified inter–molecular interactions due to the oriented mesomorphic phase, diverting a larger portion of the stress to the stronger covalent backbone of the polymer. This explanation was consistent with the largest shrinkage for the 0.4-µm fibres upon heating (54 %, Table 1), and the high Young's modulus which exceeded that of all the other fibres (2.1 GPa, Fig. 5). The more extensive initial molecular orientation due to the larger draw ratio for the 0.4-µm fibres also explained the reduced strain at break of these fibres compared with that of the 1.0-µm fibres. Extensive molecular stretching is known to lower the strain at break. The most prominent example of this is probably the drawing and preparation of ultra-high-molecular-weight polyethylene fibres (Spectra® fibres), which show only a fraction of the strain at break of the un-stretched material.[43]

Smoke Filtration

Fig. 7a and b shows one of the electrospun fibre mats before and after smoke filtration. The filtration capabilities of the mats were tested using a cigarette as the smoke source. The fibre mat/membrane was secured inside the tubular system according to Fig. 7c. The air/smoke flow was controlled via a flow rate valve (not shown) and was adjusted to expose the fibre mats to the same amount of smoke (2 mL of smoke per µg of fibre mat, at 100 mL·min^{-1}). The fibre mats turned brown immediately when subjected to the smoke (see supplementary video), and although the effectiveness of the filtration was obvious to the naked eye (Fig. 7b), additional IR spectroscopy measurements were made, see Fig. 7d. All the spectra were normalized to the absorbance of the characteristic PET bands (Fig. 3). A substantial increase in the IR-absorbance of the mat after the smoke filtration occurred in the 3000–2850 cm^{-1} range, corresponding to C-H stretching. This C-H stretching can be related to the many carcinogenic hydrocarbons that exist in tobacco smoke.[16] The additional hump shown in the 3500–3200 cm^{-1} region corresponds to the O–H stretching (possibly also N-H stretching) characteristic of alcohols, hundreds of which are identified in tobacco smoke and possibly contribute in tumorigenesis.[16] Overall the absorption of these hydrocarbons/alcohols increased as the fibre diameter decreased, *i.e.* when the specific surface area (SSA) increased. The SSA for each membrane was calculated by assuming smooth and long cylindrical fibres, shown in Table 2.

Table 2. Filtration capacity of the electrospun PET filter membranes compared to the original cigarette filter tip.

Fibre diameter	Specific surface area	Rel. mass uptake	Rel. mass uptake (after drying)	Volatile fraction
0.4 µm	7.07 m^2/g	43.7	41.5	0.049
1.0 µm	2.90 m^2/g	32.9	30.7	0.067
4.3 µm	0.67 m^2/g	26.4	23.1	0.126
Original filter tip	0.10 m^2/g	2.7	2.0	0.252

A large excess of burnt cigarette smoke was passed through each fibre mat. Mass uptakes are relative to the initial fibre mat weight. The fraction of volatile components is relative to the total mass of all absorbed substances.

The filtration capacities of the electrospun PET membranes were further evaluated by measuring the total mass uptake when a large excess of cigarette smoke was passed through each filter. The results verified that the thinner fibres (0.4 µm) contained the highest amount of absorbed smoke components (43.7 times its own weight, Table 2), the fibre mat weight-increase was ca. 2 times higher than that seen for the 4.3 µm fibres (absorbed 26.4 times its own weight). Small amounts of volatile components were absorbed in all the filters (*e.g.* water), which revealed themselves when drying the membranes in vacuum for >3 h. The amount of evaporated volatile components in the thickest fibres (4.3 µm), was 12.6 wt% of the total absorbed mass, whereas the absorbed substances in the 0.4 µm fibres contained only 4.9 wt% volatiles.

The original cellulose acetate cigarette filter tip absorbed only 2.7 times its own weight during the same treatment. In addition to the inferior filtration capacity, these much thicker fibres absorbed a larger portion of volatiles, 25.2 wt% of the absorbed matter. This can be interpreted as if the fibre mats with thick fibres and thus larger pores, had a much lower capability of trapping small solid/non-volatile particles.

Conclusions

Solution-electrospinning has been used to prepare the thinnest ever reported PET fibres obtained from recycled PET. The thermal (DSC) and the IR characteristics of the polymer were the same before and after electrospinning, neither showed any evidence of degradation in the electrospun fibres. The average fibre diameter was varied by over one order of magnitude (from 0.4 µm to 4.3 µm) by adjusting the concentration of recycled PET in the electrospinning solutions. The uniformity of the fibres depended on the feed rate of the solutions, the most uniform fibres being formed at the slowest rates. A template transfer method (TTM) was applied to carry out micromechanical tensile testing on aligned fibre mats, and it was found that the strength, strain at break, and modulus increased as the fibre diameter decreased. This resulted in a large increase in toughness of the fibres, making them useful for filtration applications. The 1.0 µm thick PET fibres displayed high strength, a high modulus and high toughness (62.5 MPa, 1.39 GPa and 65.5 $MJ \cdot m^{-3}$). The improvement in the mechanical properties originated from the formation of a completely amorphous mesomorphic phase with highly oriented PET molecules, as a result of the extensive fibre stretching and the rapid solidification of the fibres during the spinning. The molecular draw ratio was greater than 2.2 for the thinnest fibres, which was higher than that in the original PET bottle. The fibre mats were evaluated as filtration devices for air filtration of condensing hydrocarbons and particulate matter. Tobacco smoke was chosen as a model substance as it contains thousands of different particulate and vapour phase substances. IR-analysis confirmed an increased absorption efficiency of hydrocarbons and alcohols as the fibre diameter decreased. Gravimetrical measurements also showed an increased filtration capacity (especially of non-volatile particles) with decreased fibre diameter. A filtration capacity of more than 43 times the filters own weight was seen for filters with an average fibre diameter of 0.4 µm, which is significantly higher than shown for the original cigarette filter tip.

The combination of the large-scale availability of recycled PET, the electrospinning-induced formation of a toughness-enhancing internal morphology yielding ca. 30 times tougher fibre mats, and the high affinity of these PET fibre mats for air-borne hydrocarbons, also open the way for the applied use of recycled PET in a range of industrial filters. In the future we foresee that these recyclable electrospun non-woven filters develop into biodegradable materials that not only show specific absorption characteristics but also with a tailored lifespan for the intended application, *e.g.* materials based on bio-polyesters.

Acknowledgements

The UIUC Department of Chemical and Biomolecular Engineering is acknowledged for the collaborative exchange program between KTH and the University of Illinois at Urbana-Champaign. Sara Blomqvist, Samer Nameer and Amelie Hållberg are acknowledged for their assistance in the pre-screening of different solvent combinations.

Notes and references

[a] University of Illinois at Urbana-Champaign, Department of Chemical & Biomolecular Engineering, 114 Roger Adams Laboratory, MC 712, 600 South Mathews Avenue, Urbana, IL 61801, U.S.

[b] KTH Royal Institute of Technology, School of Chemical Science and Engineering, Fibre and Polymer Technology, 100 44 Stockholm, Sweden. E-mail: riander@kth.se, Tel: +46 8 7909426, Fax: +46 8 208856 or rols@kth.se, Tel: +46 8 7907637.

† Electronic Supplementary Information (ESI) available: Video of smoke adsorption testing. See DOI: 10.1039/b000000x/

1. U.S. Environmental Protection Agency, Wastes - Resource Conservation - Common Wastes & Materials - Plastics, http://www.epa.gov/osw/conserve/materials/plastics.htm, Accessed 2014-09-03.
2. V. Jankauskaitė, G. Macijauskas and R. Lygaitis, *Mater. Sci.*, 2008, **14**.
3. F. Welle, *Resources, Conservation and Recycling*, 2011, **55**, 865-875.
4. I. Grishenko, *Polyethylene terephthalate Weekly price report 13 January 2012*, ICIS Report 13.01.2012, Reed Elsevier, London, 2012.
5. A. Oromiehie and A. Mamizadeh, *Polym. Int.*, 2004, **53**, 728-732.
6. B. Veleirinho, M. F. Rei and J. A. Lopes-Da-Silva, *J. Polym. Sci., Part B: Polym. Phys.*, 2008, **46**, 460-471.
7. G. Li, Y. Zhao, M. Lv, Y. Shi and D. Cao, *Colloids Surf. Physicochem. Eng. Aspects*, 2013, **436**, 417-424.

8. F. Awaja and D. Pavel, *Eur. Polym. J.*, 2005, **41**, 1453-1477.
9. H. Rajabinejad, R. Khajavi, A. Rashidi, N. Mansouri and M. E. Yazdanshenas *Int. J. Env. Res. Public Health*, 2009, **3**, 663-670.
10. R. D. Anandjiwala and L. Boguslavsky, *Text. Res. J.*, 2008, **78**, 614-624.
11. M. A. S. Spinacé and M. A. De Paoli, *J. Appl. Polym. Sci.*, 2001, **80**, 20-25.
12. C. L. Beyler and M. M. Hirschler, *SFPE handbook of fire protection engineering*, 2002, **2**.
13. C. J. Thompson, G. G. Chase, A. L. Yarin and D. H. Reneker, *Polymer*, 2007, **48**, 6913-6922.
14. Y. Cai, H. Ke, T. Zhang, J. Dong, H. Qiao, H. Wang, Zhangfei, Q. Wei, Y. Zhao and H. Fong, *Polym. Polym. Compos.*, 2011, **19**, 773-780.
15. P. Čupr, Z. Flegrová, J. Franců, L. Landlová and J. Klánová, *Environ. Int.*, 2013, **54**, 26-34.
16. R. L. Stedman, *Chem. Rev.*, 1968, **68**, 153-207.
17. J. Phillips, B. Kluss, A. Richter and E. Massey, *Altern Lab Anim*, 2005, **33**, 239-248.
18. Z. Li and C. Wang, in *One-Dimensional nanostructures*, Springer Berlin Heidelberg, 2013, ch. 2, pp. 15-28.
19. R. L. Andersson, M. Salajkova, P. E. Mallon, L. A. Berglund, M. S. Hedenqvist and R. T. Olsson, *J. Polym. Environ.*, 2012, **20**, 967-975.
20. R. L. Andersson, A. Martínez-Abad, J. M. Lagaron, U. W. Gedde, P. E. Mallon, R. T. Olsson and M. S. Hedenqvist, *Int. J. Mol. Sci.*, 2014, **15**, 15912-15923.
21. T. Uchiyama, M. Suyama, M. M. Alam, T. Asano, S. Henning, A. Flores, F. J. Baltá Calleja and M. F. Mina, *Polymer*, 2007, **48**, 542-555.
22. Y. Kong and J. N. Hay, *Polymer*, 2002, **43**, 3873-3878.
23. H. W. Starkweather, P. Zoller, G. A. Jones and A. J. Vega, *J. Polym. Sci. Polym. Phys. Ed.*, 1982, **20**, 751-761.
24. C. Wang, M.-F. Lee and Y.-J. Wu, *Macromolecules*, 2012, **45**, 7939-7947.
25. R. E. Kagarise, *J. Chem. Phys.*, 1957, **27**, 519-522.
26. D. Papkov, Y. Zou, M. N. Andalib, A. Goponenko, S. Z. D. Cheng and Y. A. Dzenis, *ACS Nano*, 2013, **7**, 3324-3331.
27. L. Á. Córdoba, G. Martínez-Barrera, C. B. Díaz, F. U. Nuñez and A. L. Yañez, *Int. J. Polym. Sci.*, 2013, **2013**, 6.
28. Y. Rao, J. Greener, C. A. Avila-Orta, B. S. Hsiao and T. N. Blanton, *Polymer*, 2008, **49**, 2507-2514.
29. D. G. Baird and D. I. Collias, *Polymer processing – principles and design*, John Wiley and Sons, New York, 1998.
30. J. H. Lee, K. S. Lim, W. G. Hahm and S. H. Kim, *J. Appl. Polym. Sci.*, 2013, **128**, 1250-1256.
31. J. Yao, C. W. Bastiaansen and T. Peijs, *Fibers*, 2014, **2**, 158-186.
32. D. E. Bosley, *J. Appl. Polym. Sci.*, 1964, **8**, 1521-1529.
33. A. Hadjizadeh, A. Ajji and M. N. Bureau, *J. Mech. Behav. Biomed. Mater.*, 2011, **4**, 340-351.
34. R. A. X. Nunes, V. C. Costa, V. M. d. A. Calado and J. R. T. Branco, *Materials Research*, 2009, **12**, 121-125.
35. X. Jiang, S. Luo, K. Sun and X. Chen, *Express Polym Lett*, 2007, **1**, 245-251.
36. J. K. Keum and H. H. Song, *Polymer*, 2005, **46**, 939-945.
37. J. K. Keum, H.-J. Jeon, H. H. Song, J.-I. Choi and Y.-K. Son, *Polymer*, 2008, **49**, 4882-4888.
38. R. L. Andersson, V. Ström, U. W. Gedde, P. E. Mallon, M. S. Hedenqvist and R. T. Olsson, *Sci. Rep.*, 2014, **4**, 6335.
39. U. W. Gedde, *Polymer Physics*, Springer, 1995.
40. A. M. Pourrahimi, D. Liu, L. K. H. Pallon, R. L. Andersson, A. Martinez Abad, J. M. Lagaron, M. S. Hedenqvist, V. Strom, U. W. Gedde and R. T. Olsson, *RSC Advances*, 2014, **4**, 35568-35577.
41. G. D. Mihai, V. Meynen, M. Mertens, N. Bilba, P. Cool and E. F. Vansant, *J Mater Sci*, 2010, **45**, 5786-5794.
42. J. Greener, A. H. Tsou and T. N. Blanton, *Polym. Eng. Sci.*, 1999, **39**, 2403-2418.
43. J. Smook, W. Hamersma and A. Pennings, *J Mater Sci*, 1984, **19**, 1359-1373.